INSPIRO - Inovativni študentski projekti v raziskovalnem okolju
University of Nova Gorica
School of Science

Distinguishing between stars and dark stellar remnants using gravitational microlensing – followup observations of Gaia microlensing events using GoChile

Author:

Martina Larma

Mentor:

Mateusz Bronikowski, MSc

September 26, 2022

Abstract

The transient brightening of stars due to gravitational microlensing is detected regularly by surveys such as OGLE, or by the Gaia space observatory. Here we analyze two microlensing events first published as Gaia Photometric Science Alerts. We wished to calculate the masses of the two lenses, and see if they are in the range of masses of stellar black holes. We used the robotic GoChile telescope to observe one of these events, and analyzed publicly available data to model both of them. With the best fitting parameters, we were able to make an estimate of the masses of the two lenses as well as their distances and apparent magnitudes. The masses were found to be lower than the lowest observed mass of a stellar black hole, which is $3.3^{+2.8}_{-0.7}M_{\odot}$. The parameters of the lenses in both cases were found to be in agreement with stellar lenses rather than black holes.

Contents

1 Introduction

1.1 Dark matter and black holes

The effects of dark matter were first noticed as early as the late 19th century, by Lord Kelvin, who estimated the mass of the galaxy, and found it to be different from the mass of visible stars (Kelvin (1904)[15]). In the early 20th century, several notable scientists were considering the existence of this elusive form of matter, including Fritz Zwicky, who, using the virial theorem, estimated that the Coma cluster had about 400 times more mass than was visible (Zwicky (1937)[19]); he named this excess mass *dunkle Materie* or "dark matter". In the 1970s and 1980s, the first strong observational evidence for the existence of dark matter came in the form of galaxy rotation curves (e.g. Rubin et al.(1978)[12]).

The exact nature of dark matter is a still unresolved problem in physics, with several different explanations posited for candidate forms of dark matter, including baryonic, as well as hypothetical non-baryonic matter. One of the proposed forms of dark matter are the so-called massive astrophysical compact halo objects, or MACHOs. MACHOs are bodies that emit little to no radiation, drifting through interstellar space. They could be in the form of stellar remnants formed by the gravitational collapse of stars, which are black holes, neutron stars, and white dwarfs, or in the form of brown dwarfs. MACHOs could also be composed of hypothetical primordial black holes, which formed soon after the Big Bang; these black holes would be non-baryonic.

Due to the nature of their formation, the masses of stellar black holes range from a few solar masses, to several dozen solar masses. The smallest-mass black hole known so far is located in the binary system 2MASS J05215658+4359220, with a mass of 3.3 $M_\odot$ (Thompson (2019)[14]). Primordial black holes, on the other hand, could have any mass, as in the general theory of relativity, there is no constraint on the mass; however, if they had indeed formed, primordial black holes of mass lower than 10^{11} kg, or 10^{-19} $M_\odot$ would have evaporated via Hawking radiation by today.

Constraining the amount of dark matter that is found in the form of MACHOs is important as it brings us closer to solving this major problem of modern astronomy.

1.2 General relativity and gravitational lensing

The general theory of relativity, proposed by Albert Einstein in 1915, provides a description of gravity as a geometric phenomenon which arises from the curvature of space-time. One notable prediction of this theory is the bending of the light from stars passing by our Sun. An experiment was conducted in 1919, led by Frank Watson Dyson and Arthur Stanley Eddington, on the Western coast of Africa and in Brazil. The experiment required a total solar eclipse; the position of stars near the Sun were measured. This was compared to their previously measured positions during the night, when they were not near the Sun; a deflection which was measured was in agreement with Einstein's prediction of 1.75", thus confirming his general theory of relativity (Dyson et al.(1919)[3]).

Einstein also described the bending of light by other stars besides our Sun. In 1936, at the urging of R.W. Mandl, an amateur with an interest in his general theory of relativity, Einstein considered the deflection of the light of a background star due to a foreground star. He found that the image of the

star can be highly magnified if the source, the deflector, and the observer are well aligned (Einstein (1936)[4]). However, he concluded that this effect, now more broadly known as gravitational lensing, would be highly unlikely to be observed, due to the improbability of having the required alignment of the system. A year later, the Swiss astronomer Fritz Zwicky considered the lensing of and by so-called nebulae (now known as galaxies), as they are much more massive than stars, and thus their lensing is more likely to be observed. Several decades later, in 1979, the first gravitational lens was discovered (Walsh et al.(1979)[16]), in the form of two identical images of a quasar, caused by lensing from a foreground galaxy. Quasars were previously recognized as ideal candidates for gravitational lensing, due to their point-like appearance, their large distance, and their high luminosity. This phenomenon where the images formed by lensing can be resolved is known as strong lensing; today we know of several hundred such events.

Another form of gravitational lensing, named gravitational microlensing by Polish astronomer Bohdan Paczynski, describes the amplification of light coming from a lensed star. In this case, images of the star cannot be resolved, but an amplification of the source star's flux can be observed. Paczynski proposed that gravitational microlening could be used to look for dark matter in the form of MACHOs of mass $> 10^{-6}$ $M_{\odot}$ in the Galactic halo (Paczynski (1986)[9]). Normally, objects such as isolated black holes are not observable directly. However, due to the effect of gravitational lensing, the brightening of background objects passing behind these dark lenses, which emit no light of their own, can be observed.

Several groups attempted to use this method to detect MACHOs in the Milky Way. One of these was the MACHO project, active between 1992 and 1999. It monitored stars in the Large Magellanic Cloud (LMC) and in the Galactic Bulge on a regular basis, constructing light curves for over 8 million stars in the LMC and 15 million stars in the Bulge. It achieved several "firsts" in microlensing, such as the first strong detection of a microlensing star, the first real-time announcement of an ongoing micolensing event, and the first observation of parallax effects in a microlensing event. After analyzing the data, a 100% all-MACHO Milky Way halo was ruled out at the 95% confidence level for a wide range of models (C. Alcock et al.(2000)[1]). This project did not solve the dark matter problem, but it did place important upper limits on the fraction of dark matter in the form of MACHOs across a range of masses, with one possibility being that the Milky Way halo consists of about 20% MACHOs.

Another notable group is the Optical Gravitational Lensing Experiment (OGLE), which has been running a long-term variability sky survey since 1992. The main goals are the detection and classification of variable stars (pulsating and eclipsing), discovery of microlensing events, dwarf novae, and studies of the structure of the Galaxy and the Magellanic Clouds. The results of the OGLE-III monitoring of the Small Magellanic Cloud constrained the fraction of black holes in the Galactic Halo to less than 2% (Wyrzykowski et al.(2011)[18]).

1.2.1 Microlensing formalism

The standard geometry of point-lens microlensing is rather simple, with the observer (O), lens (L), and source (S) aligned. The deflection of the light by an angle α is given by the formula (Einstein (1936)[4]):

$$\alpha = \frac{4GM}{r_E c^2} \tag{1}$$

where r_E is the Einstein radius; the light arrives to the observer displaced by an angle θ_E. If the components are aligned, the source is imaged into a ring of radius r_E; if the alignment is not perfect, two images will form instead of a ring. The diagram of the standard formalism is given below.

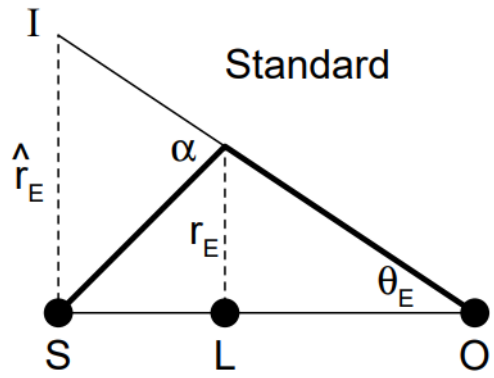

Figure 1: *The standard microlensing geometry. The deflection angle α is given by 1. The bold line shows the path of the light from the source (S) the observer (O) deflected by the lens (L). The Einstein radius r_E is shown as the dashed line going through L, while angular Einstein radius θ_E projected onto the source plane is given by $\hat{r}_E$. The image (I) is displaced from the source by θ_E. Image sourced from Gould (2000)[8].*

An alternate formalism can be developed if one inverts the standard geometry so that the Einstein radius is projected onto the observer plane instead of the source plane (Gould (2000)[8]); in this case, we can more readily see the relation between the observables $(\theta_E, \tilde{r}_E)$ and the physical quantities (M, π_{rel}), where π_{rel} is the lens-source relative parallax. The so-called "natural" geometry is presented below.

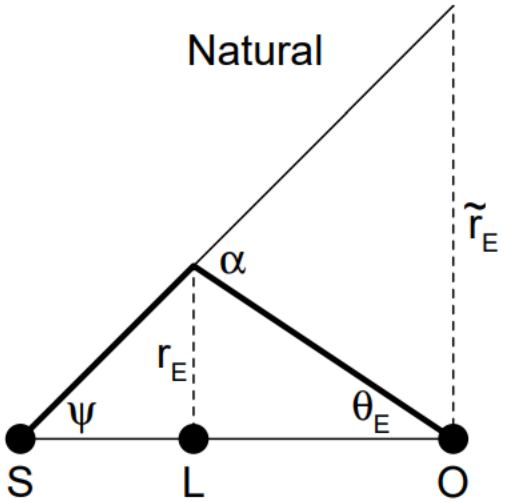

Figure 2: *The natural microlensing geometry. Similar to the image above, except that the Einstein radius is now projected onto the observer plane; the projection is labeled as $\tilde{r}_E$. Image sourced from Gould (2000)[8].*

Using the small-angle approximation, we can write the relation $\frac{\alpha}{\tilde{r}_E} = \frac{\theta_E}{r_E}$, or

$$\theta_E \tilde{r}_E = \alpha r_E = \frac{4GM}{c^2} \tag{2}$$

If we use the exterior-angle theorem, we can write the angular Einstein radius as:

$$\theta_E = \alpha - \psi = \frac{\tilde{r}_E}{d_l} - \frac{\tilde{r}_E}{d_s} = \frac{\tilde{r}_E}{d_{rel}} \tag{3}$$

where d_s and d_l are the distances to the source and the lens, respectively, with $\frac{1}{d_{rel}} \equiv \frac{1}{d_l} - \frac{1}{d_s}$. We can rewrite Eq.3 as:

$$\pi_E \theta_E = \pi_{rel}, \quad \pi_E \equiv \frac{AU}{\tilde{r}_E} \tag{4}$$

with $\pi_{rel} = \frac{AU}{d_{rel}}$, the lens-source relative parallax.

1.2.2 Microlensing and photometry

Because microlensing manifests as a change in brightness of the source being lensed, if we measure the magnitude of the event over its duration, we obtain a light curve. In the simplest scenario, where the size of the source star can be neglected, and the relative lens-souce motion is linear, we obtain the Paczynski light curve (Paczynski (1986)[9]). If we write the gravitational lensing equation in the lens's plane:

$$r^2 - r_0 r - r_E^2 = 0 \tag{5}$$

where the positions of the images are given by r, the position of the source is given by r_0, and r_E is the radius of the Einstein ring. We see that the equation has two solutions, corresponding to the two images:

$$r_{1,2} = \frac{[r_0 \pm (r_0^2 + 4r_E^2)^{1/2}]}{2} \tag{6}$$

The amplifications of the two images are given by:

$$A_{1,2} = \left| \frac{r_{1,2}}{r_0} \frac{dr_{1,2}}{dr_0} \right| = \left| \frac{r_{1,2}^4}{r_{1,2}^4 - r_E^4} \right| \tag{7}$$

Since the individual images typically cannot be resolved in the case of microlensing, we can write their total amplification as:

$$A_{1,2} = A_1 + A_2 = \frac{u^2 + 2}{u(u^2 + 4)^{1/2}} \tag{8}$$

where u $\equiv \frac{r_0}{r_E}$. If the relative motion of the source and the lens is assumed to be rectilinear, the parameter u as a function of time is given by:

$$u^2 = u_0^2 + \left(\frac{t - t_0}{t_E} \right)^2 \tag{9}$$

where t_0 is the time of the closest approach, u_0 is the impact parameter, and t_E is the Einstein timescale. Using Eq.9, we can obtain the amplification $A(u(t))$ as a function of time; this gives us the so called Paczynski curve.

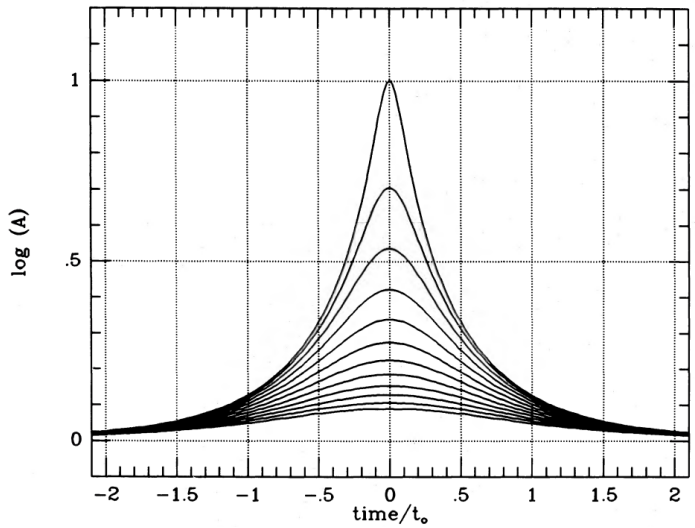

Figure 3: *Theoretical time variation of the amplification due to microlensing; events are plotted for impact parameters u_0 = 0.1, 0.2, ..., 1.1, 1.2. The largest amplification happens for the smallest impact parameter. Image sourced from Paczynski (1986)[9].*

1.2.3 Blending

Another important feature to consider is that, especially in ground based observations, we cannpt be sure that we can resolve all stars. It is possible that there are other stars next to our source star which are contributing to the total flux we observe, but which are not being lensed. Hence we define the flux observed from the target for a specific telescope and filter as:

$$F(t) = F_S A(u(t)) + F_B \tag{10}$$

where F_S is the intrinsic source flux, and F_B is the background flux coming from unresolved stars near the source. We can define the fraction of light that is coming from the source star as:

$$f_S = \frac{F_S}{F_S + F_B} \tag{11}$$

so that the amount of blended light is then $f_B = 1 - f_S$.

In fact, the background flux can also be coming from the lens itself, in the case that it is also a star. Thus, the blending fraction is very important when modelling microlensing events in order to estimate the amount of light which is coming from the lens, to determine if it is a star or a dark lens.

1.2.4 Mass and distance

If we consider Equations 2 - 4, we can easily obtain an expression for the mass of the lens as:

$$M = \frac{\theta_E}{\kappa \pi_E} = \frac{\mu_{rel} t_E}{\kappa \pi_E} \tag{12}$$

where $\kappa = \frac{4G}{c^2 AU}$, and $\mu_{rel} = \mu_E \theta_E$, with $\mu_E = \frac{1}{t_E}$. With Eq.12, we can simply calculate the mass of the lens by fitting the observed data to the model and estimating the microlensing parameters. Eq.12 gives us a more intuitive understanding of the observable microlensing parameters in relation to physical parameters of the lens, and as such is a very powerful tool.

If we now consider Eq.4, using relations $\pi_{rel} = \frac{AU}{d_{rel}}$ and $\frac{1}{d_{rel}} = \frac{1}{d_l} - \frac{1}{d_s}$, we can show that

$$\pi_E t_E \mu_{rel} = \frac{AU}{d_L} - \frac{AU}{d_S} \tag{13}$$

We can see that, provided that we know the distance to the source object, we can calculate the distance to the lens using Eq.13. With two simple equations, we are able to calculate two very important physical parameters, which help us characterize the nature of the lens.

We can use these parameters to further investigate the properties of the lens. If the lens is a main sequence star, as the majority of stars are, we can predict the magnitude that a main sequence star of such a mass and distance should have. We do this by checking what color, or difference of absolute magnitudes in certain filters, a main sequence star of a specified mass has. We refer to the tabulation[1] presented by Pecaut and Mamajek (2013)[10]. Then, we use the estimated distance of the lens to calculate the apparent magnitude of that star in a given band. We can compare this apparent magnitude to the magnitude that we have observed. In most cases, the system will have a higher apparent magnitude than the estimated apparent magnitude of the main sequence lens, and not much more can be said about it. However, in the case that the system has a lower apparent magnitude than the one calculated for the main sequence lens, the situation gets interesting, as we seem to be missing the expected contribution from a bright lens; this would imply that we are dealing with a dark lens. This is how black holes can be found using microlensing.

2 Methods and observations

2.1 Targets

For this project, I decided to perform follow-up observations on a microlensing event first detected on 27.02.2022. by the Gaia space observatory. The event, named Gaia22awa[5], was published by Gaia Science Alerts, with an alerting magnitude of 14.59, compared to its historic magnitude of 15.11. The aim of the observations was to follow the developing event for as long as possible in order to obtain photometric information on it, which could be used to fit a light curve and calculate the parameters of the event. Another event, Gaia22bhc[6], was observed, although due to its proximity to the Galactic Center it was not possible to extract accurate photometry, as the field it was in was very crowded. Instead, a different event named Gaia22bpl[7] was chosen for modeling alongside Gaia22awa, as it had a good amount of data available, although no follow-up observations were performed by me. Gaia22bpl was first detected on 14.04.2022., with an alerting magnitude of 12.15, compared to its historic magnitude of 12.70.

2.2 Observations

The observations were performed using the GoChile GoT1 telescope. The GoChile is a Slovenian robotic telescope run by the University of Nova Gorica and the astronomical magazine Spika. It is located in the southern part of the Atacama desert, at an altitude of 1560 m. GoT1 is a 400 mm Ritchey-Chrétien reflecting telescope. The observations were performed over the span of three

[1]Online version from 16.04.2022. at `https://www.pas.rochester.edu/~emamajek/EEM_dwarf_UBVIJHK_colors_Teff.tx`

months, starting at the beginning of May, observing every other night. Images were taken in three filters available, which are R, G, and B; the exposure time was 10 minutes, with two exposures taken every observing night. Below is a table displaying the dates of all of the successful observations of Gaia22awa. There were many nights in June and July when observations were not possible due to the poor weather conditions at the observing location. Additional observations needed to be performed in August and September to improve the model, as it wasn't possible to know when the event would return to the baseline. In fact, as of 16.09.2022., it had not yet returned to the baseline magnitude, meaning additional observations could potentially change the values of the fitted parameters.

#	Observation date
1	04.05.
2	06.05.
3	10.05.
4	14.05.
5	16.05.
6	18.05.
7	20.05.
8	22.05.
9	24.05.
10	26.05.

#	Observation date
11	28.05.
12	07.06.
13	09.06.
14	11.06.
15	13.06.
16	17.06.
17	19.06.
18	18.07.
19	24.07.
20	19.08.

#	Observation date
21	20.08.
22	21.08.
23	22.08.
24	23.08.
25	24.08.
26	25.08.
27	12.09.
28	13.09.
29	16.09.

Table 1: *Table showing the dates of all successful observations for Gaia22awa.*

2.3 Image reduction

The first step in the analysis of our data was the reduction of the astronomical images. This was done in order to reduce the noise in the images. The images were calibrated using AstroPixelProcessor, a software designed for processing astronomical images. The calibration frames used were dark, bias, and flat images taken during the observing nights, combined to make respective master frames, and applied to the light images.

The bias voltage is a constant offset voltage applied to the capacitor of the CCD detector before analog-to-digital converstion. The consequence of this voltage is that even if the pixel does not contain photo-electrons, the ADC will return the value of a few hundred counts. This is done intentionally, so as to avoid negative counts. However, this means our images had to be corrected for this bias voltage before doing any photometry. In order to obtain the bias level, a series of images with zero exposure time was taken.

The second effect we had to take into account were the thermally excited electrons, which produce the same effect as photo-electrons, and are therefore indistinguishable from them. This means we also had to subtract the dark current (thermal exictation of electrons) from our science images. In order to do this, we took long exposures with the shutter closed, so that no photons reach the CCD detector. Since the bias voltage is still present, we first subtracted the master bias frame from the dark frames. Then, the master dark frame was subtracted from each of our science images.

The final thing we needed to do to reduce the astronomical images was to flat-feld them. Several effects combine to mean that the count level can vary significantly across an image, even when observing a uniformly illuminated light source. This means that the read-out is not uniform. One of the reasons for this is vignetting, which is an issue with Newtonian telesopes. If the secondary mirror is not exactly the right size to fit the beam produced by an on-axis source, some fraction of the beam produced by an off-axis source will miss the secondary mirror. This light will then be lost, and off-axis sources will appear dimmer than on-axis sources. Another issue is the fact that not each pixel in a CCD is exactly the same size, which produces a grain-like effect. Dust on the window of the CCD or on the filters can also produce dark donut-like effects. This is why we had to correct our images for these effects. We did this by taking several flat frames at dawn, when the sky is approximately uniformely illuminated. The final science images are obtained by dividing the science images with the master flats.

2.4 Photometry

The images were uploaded to Black Hole TOM[2] (BH-TOM), which is a website designed with the purpose of viewing and sharing observational photometric and spectroscopic data, with a focus on candidate dark lens events. Due to the filters used during observations not being standard, they needed to be assigned to standard filters used by various surveys. This was done in order to ensure that all of the data collected by various observatories can be used together. We assigned several different standard filters when extracting the photometry for each of the filters used, and checked how well the extracted instrumental magnitudes matched with catalog magnitudes for each case, trying to reduce scatter of the points. For the case of Gaia22awa, the R frames were standardized to the Pan-STARRS1 (PS1) r filter, while the G frames were standardized to PS1 g filter; the B frames were assigned to the APASS B filter. Photometry was extracted from the images using BH-TOM, which allows users access to every obsever's data for a specific target. Due to this, photometric data was automatically collected for my data, the Gaia data, as well as any additional data gathered by other observers; this feature makes modeling of the event easier.

2.5 MulensModel

After the photometric data was downloaded from the BH-TOM, it was modelled using the MulensModel[2] package; this is a software package developed for modelling microlensing events (Poleski and Yee (2019)[11]). It generates a light curve for specified parameters, with the ability to fit the curve to a data set. It calculates the χ^2 value for the fit. It can model point or binary lenses, single or binary source stars, as well as take into account several effects, namely finite source effect, parallax, binary lens orbital motion, and different parameterizations of the models. In my analysis, several different models were considered; namely models with or without parallax, as well as models including blending, or fixing blending to not be present. The parameters that were fitted for were t_0, u_0, t_E, $\pi_{E,N}$, and $\pi_{E,E}$, as well as the blending fraction for cases in which the blending was considered to be present. For each of these four combinations of models, the obtained parameters were used to initialize an MCMC sampler using the Python emcee package. MCMC was used to sample the parameter space and find the parameters which minimize the χ^2 value, maximizing the likelihood function. After performing this for the 2 initial parallax models, another 2 fits were performed using the impact parameter of the

[2]GitHub repository available at `https://github.com/rpoleski/MulensModel`

opposite sign, i.e. by setting u_0 = -$u_{0,fit}$. This was done for both Gaia22awa and Gaia22bpl. The results of these fits are presented in the next section. After obtaining the parameters of the events, equations 12 and 13 were used to estimate the mass of the lens and the distance to it, while making some assumptions about the source, which will be discussed in the next section. Then, we can compare the observed magnitude of the event with the expected apparent magnitude of a MS star of a given mass at a given distance given by Pecaut and Mamajek (2013)[10]. If the apparent magnitude of the system is lower than the expected apparent magnitude of the lens, we can say something about the darkness of the lens.

3 Results and discussion

3.1 Relative proper motion and distance

As is apparent from equations 12 and 13, in order to calculate the mass of the lens and the distance to it, we need to know the relative proper motion between the lens and the source, as well as the distance to the source. We need to make some assumptions about the properties of the lenses and the sources. We assume that the lenses are located in the galactic disk and follow the disk's distribution of velocity and density, and we assume that the sources are in the bulge with the bulge's distribution of velocities. The most likely value of the relative proper motion can be calculated (e.g Wyrzykowski et al. (2016)[17]). For our purposes, we adopt the values of $\mu_L = 4 \pm 2$ mas/yr for lenses in the disk, and $\mu_S = 0 \pm 2$ mas/yr for sources in the bulge, giving a relative proper motion of $\mu_{LS} = 4.0 \pm 2.8$ mas/yr. In order to find the distance to the lens, we also need a constraint on the distance to the source; in our calculations, it was fixed to $D_S = 8$ kpc, as that is the distance to the galactic center. With these assumptions, it is possible to set limits on the properties of the lenses.

3.2 Gaia22awa

Gaia22awa was modeled using the MulensModel, and the parameters were calculated using MCMC with 75 walkers and 2000 steps. The parameters for blending did not converge, so this event was modeled assuming no blending (i.e. $f_S = 1$). We show an example of the best fitted model for the case of a negative impact parameter, plotted only with the data gathered using GoChile and the Gaia data for the event.

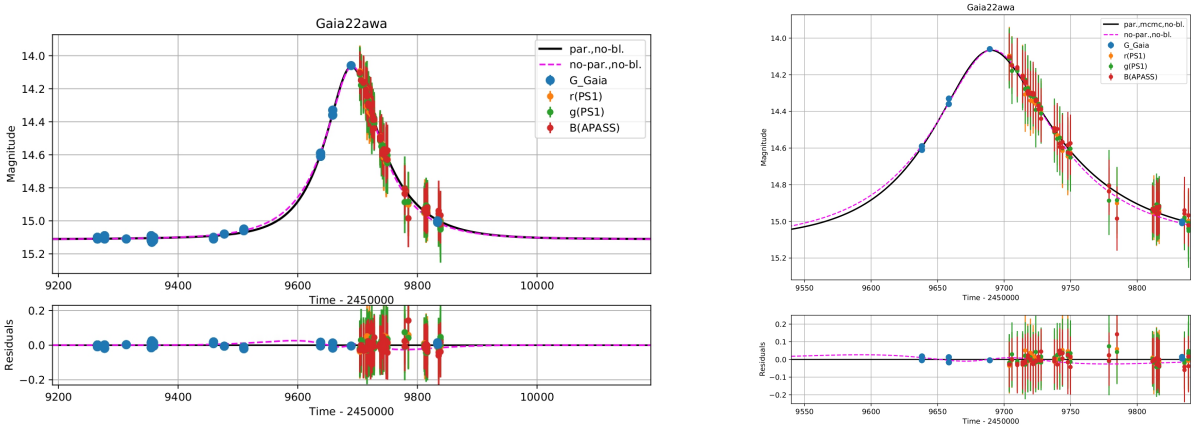

Figure 3: *The top left plot shows the model found for Gaia22awa, when considering a negative solution for u_0 without blending, along with the data collected using GoChile and the Gaia data. The dashed line shows the model which doesn't include the parallax effect, while the full black line shows the model with the parallax. Data points with included errorbars are plotted in different colours. The plot on the top right shows the same model zoomed in around the peak of the light curve. The bottom plot in both cases shows the residuals of the model.*

As we can see in the figure above, there is a slight but still noticeable difference between the models with and without the parallax effect; the parallax effect needs to be taken into account in this event. We also note that the event has not yet finished, as it has not yet returned to the baseline magnitude; further monitoring of this event will be necessary in order to model it more accurately. At the time of writing of this report, the latest data come from the night of 16.09.

The best fitting parameters for the positive and negative solutions of the impact parameters are presented in the table below.

	t_0 [JD]	u_0	t_E [d]	$\pi_{E,N}$	$\pi_{E,E}$	χ^2/n_{dof}
$u_0 > 0$	$2459690.10^{+0.32}_{-0.32}$	$0.405^{+0.002}_{-0.002}$	$91.21^{+3.94}_{-3.75}$	$-0.068^{+0.081}_{-0.072}$	$0.093^{+0.015}_{-0.016}$	0.648
$u_0 < 0$	$2459690.08^{+0.32}_{-0.31}$	$-0.405^{+0.001}_{-0.001}$	$86.76^{+0.78}_{-0.71}$	$-0.013^{+0.027}_{-0.027}$	$0.079^{+0.011}_{-0.011}$	0.648

Table 2: *Table presenting the best fitting parameters for the two configurations considered for Gaia22awa.*

As we can see from Table 2, the results are noticeably different for the parallaxes of the two models, but owing to the large uncertainties on them, they are in agreement with one another.

Mass, distance, and apparent magnitude

We used the best fitting parameters for both models to calculate the mass of the lens and the distance to it, with the assumptions described in the previous subsection. The results of these calculations are presented in the table below, along with their uncertainties.

	M_L [$M_\odot$]	D_L [kpc]
$u_0 > 0$	$1.06^{+0.88}_{-0.85}$	$4.16^{+0.39}_{-0.38}$
$u_0 < 0$	$1.44^{+1.04}_{-1.04}$	$4.94^{+0.27}_{-0.27}$

Table 3: *Table presenting the calculated mass and distance for the lens in the Gaia22awa event, presented along with their uncertainties.*

We can see from Table 3 that the lens has a mass lower than the minimum theoretical mass of a stellar black hole, under the condition that our assumptions about the relative proper motion and the distance to the source are valid. Using the table from Pecaut and Mamajek (2013)[10], we can make an estimate on the apparent magnitude of the lens, which we assume to be a main sequence star of mass M_L at a distance D_L for the purpose of this demonstration. Under these assumptions, we can find the minimum and maximum apparent magnitude in Gaia G filter, using the limiting values of the calculated mass and distance. We find that the apparent magnitude ranges from 24.8 mag to 13.5 mag for the lens in this event, compared with the baseline observed magnitude in Gaia G, which is 15.11 mag. The lower end of the range does not tell us much, as the light coming from the lens would

be embedded into the light of the source; the upper limit on the magnitude is of some interest, as it is almost two orders of magnitude brighter than the baseline magnitude of the event. If this estimate is correct, that would mean we are not seeing the expected light from the lens; it could imply a dark lens of mass lower than the theoretical minimum mass of a black hole, which would correspond to a neutron star. However, this cannot be said with much certainty, due to the assumptions which needed to be made. It is more likely that the lens is a faint stellar lens.

3.3 Gaia22bpl

Gaia22bpl was modeled using the MulensModel package, for the four combinations mentioned in the previous section. Afterwards, the MCMC algorithm was used to more precisely determine its parameters, as well as to take into account the second solution for u_0 = -$u_{0,fit}$.

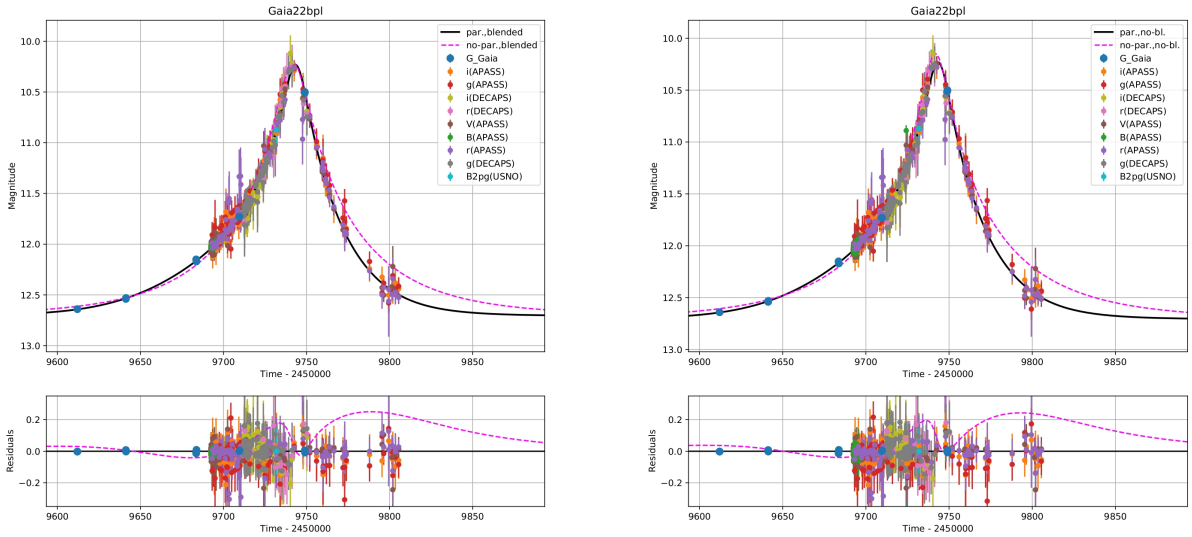

Figure 4: *The top left plot shows the model found for Gaia22bpl, when considering blending and a positive solution for u_0, along with all of the available data. The dashed line shows the model which doesn't include the parallax effect, while the full black line shows the model with the parallax. Data points with included errorbars are plotted in different colours. The plot on the top right shows the model found for Gaia22bpl when not taking blending into account, using the positive solution for u_0, along with all of the available data. The plots are zoomed in around the peak of the event. The bottom plot in both cases shows the residuals of the two models.*

It is easily visible in Fig.4 that the data points lie much closer to the parallax model than they do to the model without it; clearly the parallax effect plays a role in this event. If we consider the models with included blending versus the plots which were modeled assuming no blending, there isn't a discernible difference to the naked eye. Indeed, the parameters obtained for these two cases are very similar. This means that the calculations of the mass and distance do not depend on the amount of blending in this case, as the difference was minimal. We will present the obtained best fitting parameters in a table below

		t_0 [JD]	u_0	t_E [d]	$\pi_{E,N}$	$\pi_{E,E}$	χ^2/n_{dof}
Blending	$u_0 > 0$	$2459743.39^{+0.11}_{-0.11}$	$0.10^{+0.09}_{-0.09}$	$67.78^{+4.77}_{-4.01}$	$-0.51^{+0.01}_{-0.01}$	$0.36^{+0.04}_{-0.04}$	3.238
	$u_0 < 0$	$2459743.29^{+0.11}_{-0.11}$	$-0.09^{+0.01}_{-0.01}$	$80.46^{+8.07}_{6.51}$	$-0.50^{+0.008}_{-0.008}$	$0.37^{+0.05}_{-0.04}$	3.233
No blending	$u_0 > 0$	$2459743.37^{+0.10}_{-0.10}$	$0.10^{+0.001}_{-0.001}$	$67.67^{+0.38}_{-0.38}$	$-0.51^{+0.009}_{-0.009}$	$0.36^{+0.01}_{-0.01}$	3.275
	$u_0 < 0$	$2459743.19^{+0.10}_{-0.09}$	$-0.10^{+0.001}_{-0.001}$	$70.29^{+0.48}_{-0.48}$	$-0.51^{+0.008}_{-0.008}$	$0.44^{+0.01}_{-0.01}$	3.276

Table 4: *Table presenting the best fitting parameters for four different models of Gaia22bpl, along with their respective uncertainties.*

We can see that there isn't much variation among the parameters for the different configurations of the model; the parameter which changes the most noticeably is the Einstein crossing time, between the positive and negative solution of the impact parameter. We also present the fitted fluxes and blending fractions obtained for each of the different filters used.

	$u_0 > 0$		$u_0 < 0$	
	mag_0	f_{source}	mag_0	f_{source}
G (Gaia)	12.70	0.99	12.71	0.83
i (APASS)	12.16	1.01	12.19	0.9
g (APASS)	13.66	1.06	13.69	0.94
i (DECAPS)	12.16	0.91	12.18	0.80
r (DECAPS)	12.53	0.95	12.57	0.85
V (APASS)	13.03	0.99	13.07	0.89
B (APASS)	15.60	6.21	15.76	6.17
r (APASS)	12.55	0.94	12.59	0.85
g (DECAPS)	12.69	1.12	13.77	1.06
B2pg (USNO)	13.25	0.84	13.39	0.86

Table 5: *Table presenting the fitted values of the magnitude and flux of Gaia22bpl in all of the different filters for the case of blending.*

Mass, distance, and apparent magnitude

Using equations 12 and 13, we calculated the distance to the lens and its mass, with the assumptions discussed in the previous subsection 3.1. We present the results of these calculations along with their uncertainties in the table below.

		M_L [$M_\odot$]	D_L [kpc]
Blending	$u_0 > 0$	$0.14^{+0.10}_{-0.10}$	$1.69^{+0.56}_{-0.56}$
	$u_0 < 0$	$0.17^{+0.12}_{-0.12}$	$1.47^{+0.58}_{-0.58}$
No blending	$u_0 > 0$	$0.14^{+0.12}_{-0.12}$	$1.69^{+0.56}_{-0.56}$
	$u_0 < 0$	$0.14^{+0.09}_{-0.09}$	$1.55^{+0.57}_{-0.57}$

Table 6: *Table presenting the calculated mass and distance for the lens in the Gaia22bpl event, presented along with their uncertainties.*

As we can see from Table 6, the physical parameters of the lens are in agreement with each

other for all four configurations. We can also note that the mass of the lens is again considerably lower than the lowest measured mass of a black hole. We use the calculated mass and distance to estimate the expected apparent magnitude of a MS star at the distance of the lens; we find it to be between 31.7 mag and 20.6 mag in Gaia G, making it far fainter than the baseline of the event, which is at 12.7 mag for the same filter. Therefore, we cannot expect to distinguish the light coming from the lens from the total light of the event; due to its low mass, however, we expect the lens to be a stellar object.

4 Conclusion

Microlensing is a powerful tool for astronomy. It is the only technique for detecting isolated black holes, and it has already proven successful in this aspect (Sahu et al.(2022)[13]), although it is not the most reliable method, due to its inherent randomness. That is why large-scale sky surveys, capable of detecting and reporting variability in real time are important, along with resources for ground-based detailed follow-up observations. By following an event for several months, I was able to gather data to model it, but it would not have been possible without the publically available, crowdsourced data provided by observers from all over the world, gathered on the BH TOM website. With this data, I modeled two events, and was able to very simply calculate the physical parameters of the lensing objects, which would normally not be obtainable. This process allows us to look for black holes or other stellar remnants, which cannot be observed otherwise. In the case of the events I have modeled, they are most likely to be due to stellar lenses rather than dark ones. This was still a very valuable experience, as this process can be performed on a larger scale to identify potential dark lenses; the number of dark lensing candidates can be used to constrain the amount of dark matter present in the Galaxy in the form of MACHOs.

5 Figures

Here we present the best fitting models fitted by MCMC along with cornerplots for both events.

5.1 Gaia22awa

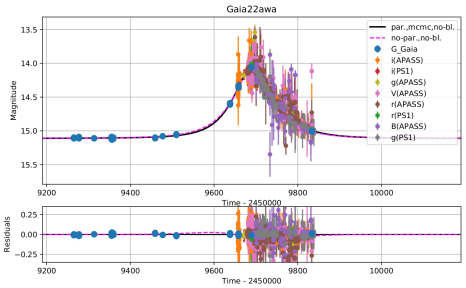

(a) *Best model of Gaia22awa with* $u_0 > 0$.

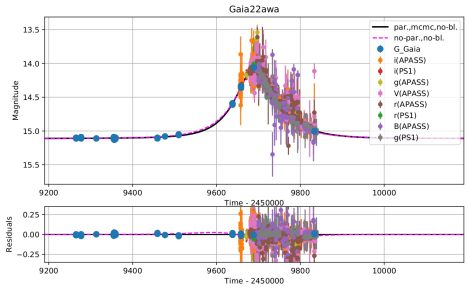

(b) *Best model of Gaia22awa with* $u_0 < 0$.

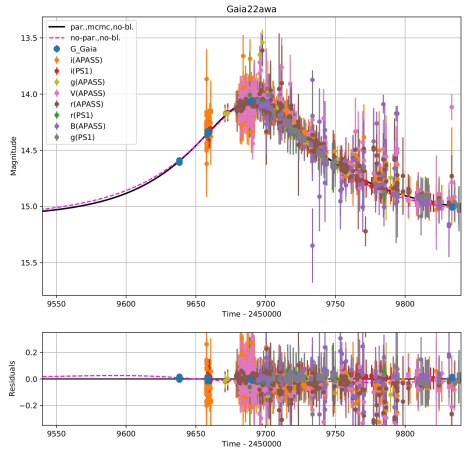

(a) *Zoomed in model with* $u_0 > 0$.

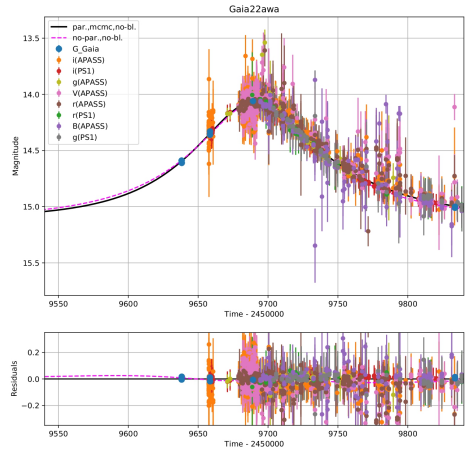

(b) *Zoomed in model with* $u_0 < 0$.

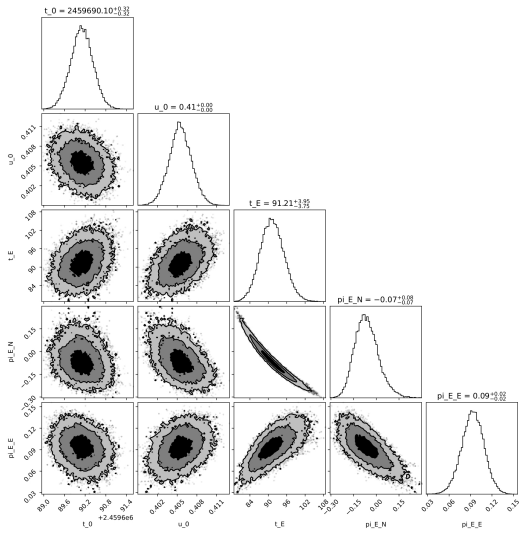

(a) *Cornerplot for the parameters with* $u_0 > 0$.

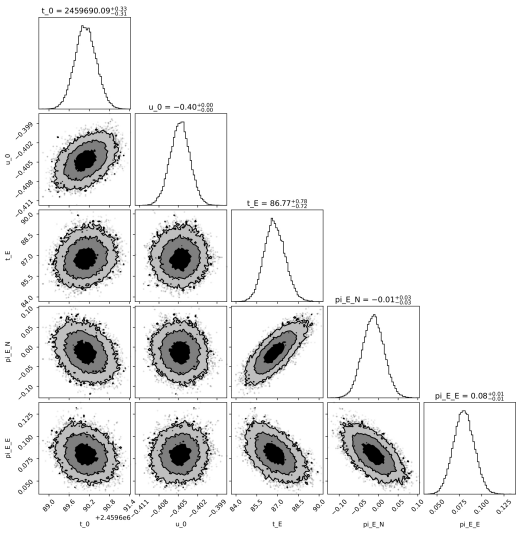

(b) *Cornerplot for the parameters with* $u_0 < 0$.

5.2 Gaia22bpl, no blending

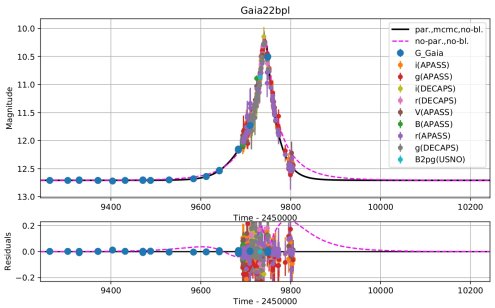

(a) *Best model of Gaia22bpl with no blending,* $u_0 > 0$.

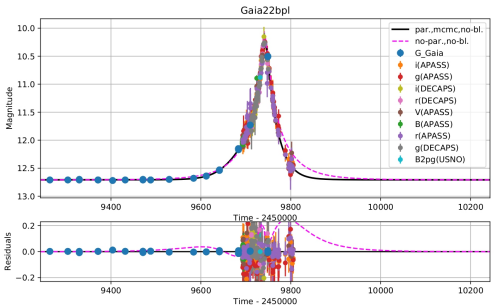

(b) *Best model of Gaia22bpl with no blending,* $u_0 < 0$.

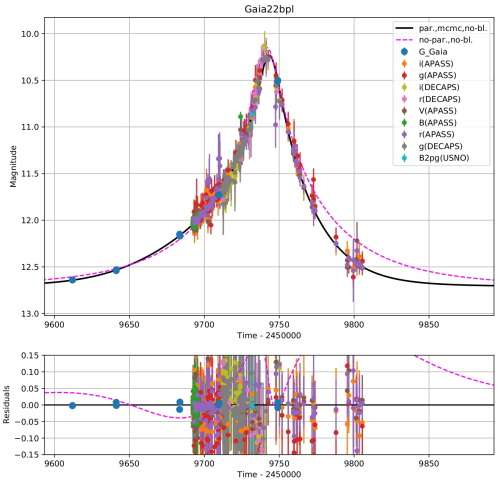

(a) *Zoomed in model with no blending,* $u_0 > 0$.

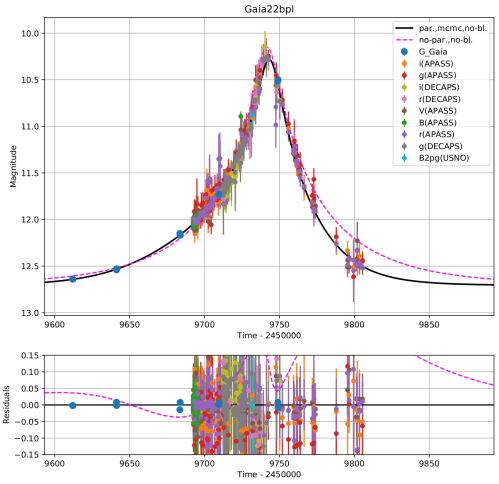

(b) *Zoomed in model with no blending,* $u_0 < 0$.

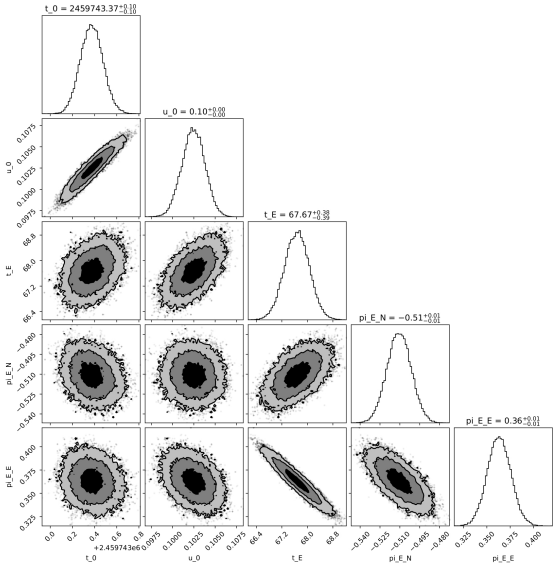

(a) *Cornerplot for the parameters with* $u_0 > 0$.

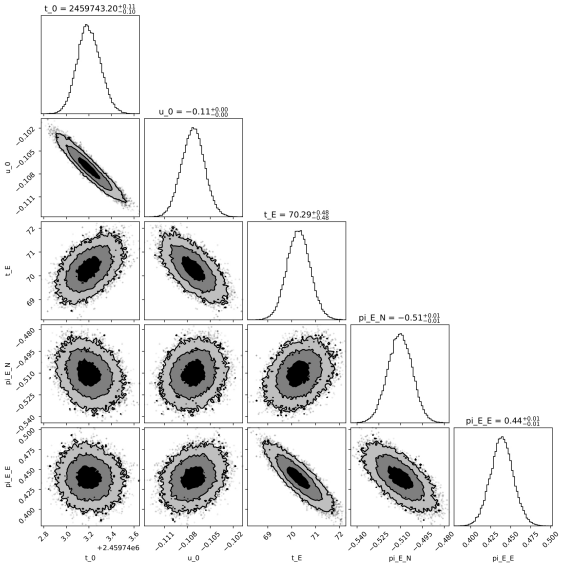

(b) *Cornerplot for the parameters with* $u_0 < 0$.

5.3 Gaia22bpl, blending included

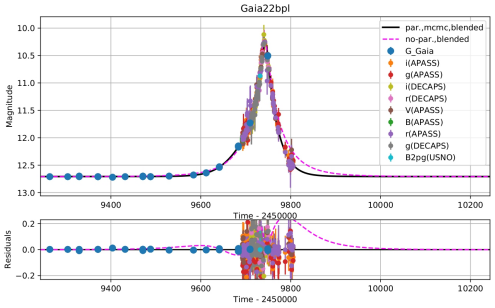

(a) *Best model of Gaia22bpl with blending,* $u_0 > 0$.

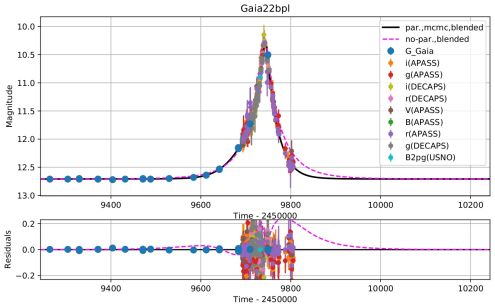

(b) *Best model of Gaia22bpl with blending,* $u_0 < 0$.

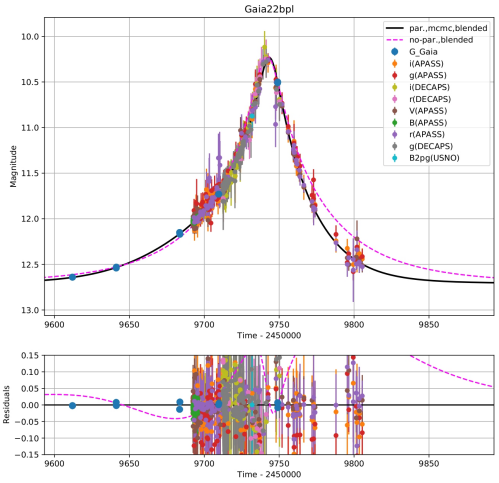

(a) *Zoomed in model with blending,* $u_0 > 0$.

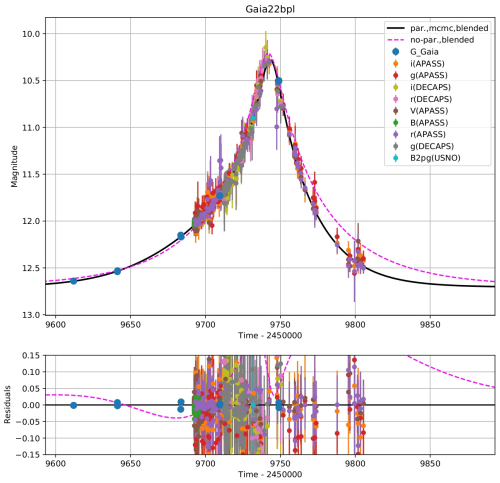

(b) *Zoomed in model with blending,* $u_0 < 0$.

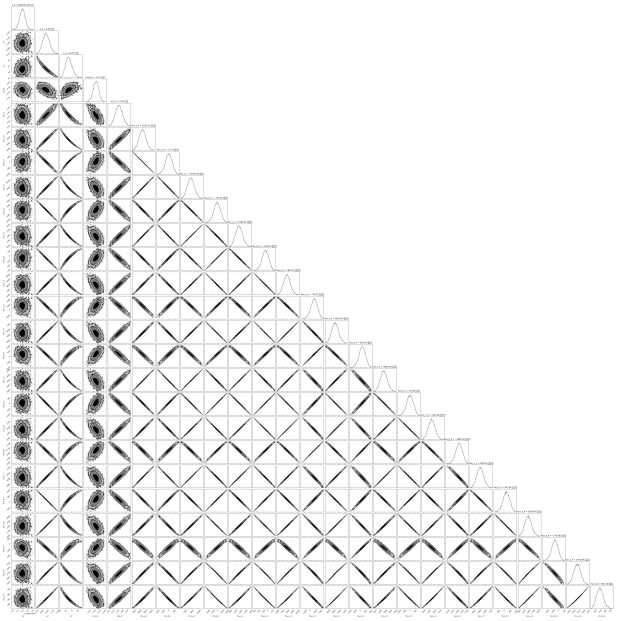

(a) *Cornerplot for the parameters with* $u_0 > 0$.

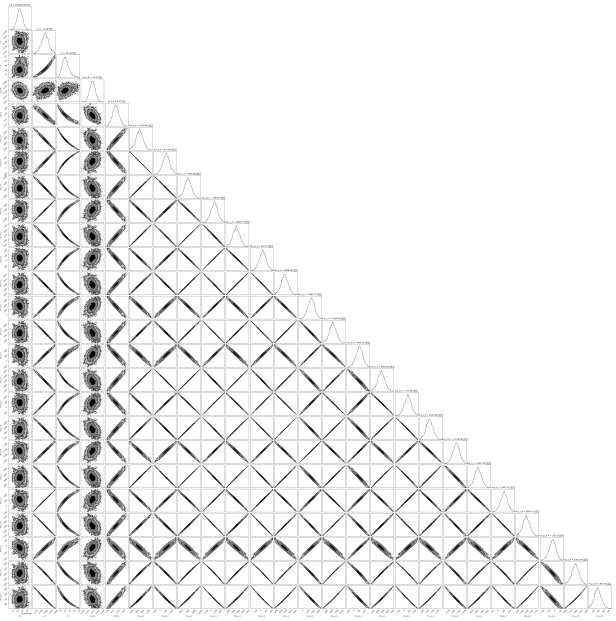

(b) *Cornerplot for the parameters with* $u_0 < 0$.

References

[1] C. Alcock et al. "The MACHO Project: Microlensing Results from 5.7 Years of Large Magellanic Cloud Observations". In: *The Astrophysical Journal* 542.1 (Oct. 2000), pp. 281–307. DOI: 10.1086/309512.

[2] *BHTOM*. URL: https://bh-tom.astrolabs.pl/.

[3] F.W. Dyson, A.S. Eddington, and C. Davidson. "A determination of the deflection of light by the sun's gravitational field, from observations made at the total eclipse of May 29, 1919". In: *Philosophical Transactions of the Royal Society of London. Series A, Containing Papers of a Mathematical or Physical Character* 220.571-581 (Jan. 1920), pp. 291–333. DOI: 10.1098/rsta.1920.0009.

[4] Albert Einstein. "Lens-Like Action of a Star by the Deviation of Light in the Gravitational Field". en. In: *Science* 84.2188 (Dec. 1936), pp. 506–507. DOI: 10.1126/science.84.2188.506.

[5] *Gaia22awa*. URL: http://gsaweb.ast.cam.ac.uk/alerts/alert/Gaia22awa/.

[6] *Gaia22bhc*. URL: http://gsaweb.ast.cam.ac.uk/alerts/alert/Gaia22bhc/.

[7] *Gaia22bpl*. URL: http://gsaweb.ast.cam.ac.uk/alerts/alert/Gaia22bpl/.

[8] Andrew Gould. "A Natural Formalism for Microlensing". In: (2000). DOI: 10.48550/ARXIV.ASTRO-PH/0001421. URL: https://arxiv.org/abs/astro-ph/0001421.

[9] B. Paczynski. "Gravitational microlensing by the galactic halo". In: *The Astrophysical Journal* 304 (May 1986), p. 1. DOI: 10.1086/164140.

[10] Mark J. Pecaut and Eric E. Mamajek. "Intrinsic colors, temperatures, and bolometric corrections of pre-main-sequence stars". In: *The Astrophysical Journal Supplement Series* 208.1 (Sept. 2013), p. 9. DOI: 10.1088/0067-0049/208/1/9. URL: https://iopscience.iop.org/article/10.1088/0067-0049/208/1/9.

[11] R. Poleski and J. C. Yee. "Modeling microlensing events with MulensModel". In: *Astronomy and Computing* 26 (Jan. 2019), p. 35. DOI: 10.1016/j.ascom.2018.11.001. URL: https://ui.adsabs.harvard.edu/abs/2019A&C....26..35P/abstract.

[12] V. C. Rubin, W. K. Ford Jr., and N. Thonnard. "Extended rotation curves of high-luminosity spiral galaxies. IV. Systematic dynamical properties, Sa -> Sc." In: *The Astrophysical Journal* 225 (Nov. 1978), pp. L107–L111. DOI: 10.1086/182804.

[13] Kailash C. Sahu et al. "An Isolated Stellar-Mass Black Hole Detected Through Astrometric Microlensing". In: *The Astrophysical Journal* 933.1 (July 2022). arXiv:2201.13296 [astro-ph], p. 83. DOI: 10.3847/1538-4357/ac739e. URL: http://arxiv.org/abs/2201.13296.

[14] Todd A. Thompson et al. "A noninteracting low-mass black hole–giant star binary system". In: *Science* 366.6465 (Nov. 2019), pp. 637–640. DOI: 10.1126/science.aau4005.

[15] William Thomson Baron Kelvin. *Baltimore Lectures on Molecular Dynamics and the Wave Theory of Light*. 1st ed. Cambridge University Press, May 2010. ISBN: 9781108007672 9780511694523. DOI: 10.1017/CBO9780511694523.

[16] D. Walsh, R. F. Carswell, and R. J. Weymann. "0957 + 561 A, B: twin quasistellar objects or gravitational lens?" In: *Nature* 279.5712 (May 1979), pp. 381–384. DOI: 10.1038/279381a0.

[17] L. Wyrzykowski et al. "Black Hole, Neutron Star and White Dwarf Candidates from Microlensing with OGLE-III". In: *Monthly Notices of the Royal Astronomical Society* 458.3 (May 2016). arXiv:1509.04899 [astro-ph], pp. 3012–3026. DOI: 10.1093/mnras/stw426. URL: http://arxiv.org/abs/1509.04899.

[18] L. Wyrzykowski et al. "The OGLE view of microlensing towards the Magellanic Clouds - IV. OGLE-III SMC data and final conclusions on MACHOs: The OGLE-III view of microlensing towards the SMC". In: *Monthly Notices of the Royal Astronomical Society* 416.4 (Oct. 2011), pp. 2949–2961. DOI: 10.1111/j.1365-2966.2011.19243.x.

[19] F. Zwicky. "On the Masses of Nebulae and of Clusters of Nebulae". In: *The Astrophysical Journal* 86 (Oct. 1937), p. 217. DOI: 10.1086/143864.